Secondary structure and dosage of soluble and membrane proteins by attenuated total reflection Fourier-transform infrared spectroscopy on hydrated film

ARTICLE · SEPTEMBER 1990

DOI: 10.1111/j.1432-1033.1990.tb19354.x

3 AUTHORS, INCLUDING:

Erik Goormaghtigh

Université Libre de Bruxelles

165 PUBLICATIONS **4,724** CITATIONS

SEE PROFILE

Jean-Marie Ruysschaert

Université Libre de Bruxelles

462 PUBLICATIONS **11,786** CITATIONS

SEE PROFILE

Eur. J. Biochem. *193*, 409–420 (1990)

Secondary structure and dosage of soluble and membrane proteins by attenuated total reflection Fourier-transform infrared spectroscopy on hydrated films

Erik GOORMAGHTIGH, Véronique CABIAUX and Jean-Marie RUYSSCHAERT

Laboratoire de Chimie Physique des Macromolécules aux Interfaces, Université Libre de Bruxelles, Belgium

(Received February 19/June 6, 1990) – EJB 90 0176

Attenuated total reflection Fourier-transform infrared spectroscopy of thin hydrated films of soluble and membrane protein included in a phospholipid bilayer is shown to provide useful information as to the secondary structure of the protein. The analysis of the amide I band of deuterated samples by Fourier self-deconvolution followed by a curve fitting was performed by a new procedure in which all the input parameters are generated by the computer rather than by the investigator. The results of this analysis provide a correct estimation of the α-helix and β-sheet structure content with a standard deviation of 8.6% when X-ray structures are taken as a reference. We also show that the orientation of the different secondary structures resolved by the Fourier self-deconvolution/curve-fitting procedure and of the phospholipid acyl chains can be simultaneously evaluated for membrane proteins reconstituted in a lipid bilayer. Of special interest for reconstitution of membrane proteins, the lipid/protein ratio can be accurately and quickly determined from the infrared spectrum.

Among the spectroscopic techniques currently used for the determination on secondary structures of proteins and peptides (circular dichroism, NMR, X-ray diffraction analysis, etc.) infrared spectroscopy has recently become a prominent one. Although its potential usefulness has been recognized for some time [1, 2], the recognition of the different components of conformation-sensitive amides bands (particularly amide I band) was difficult due to the resulting overlap of bands originating from the different secondary structures such as α-helix, β-sheet, β-turns and random. Pointing out the different components of amide I has been made possible by the advent of numerical analysis of the spectra. The computed second and fourth derivatives [3, 4] for instance replace a broad featureless band by peaks of well-resolved components. More recently, the use of Fourier self-deconvolution has provided the same type of result. The advantage of Fourier self-deconvolution is that it does not change the integrated areas of the different components of the amide envelope [5]. It must be noted that the Fourier self-deconvolution does not achieve an actual resolution enhancement but rather enhances selected frequencies of the spectrum. The actual resolution of the spectrum is defined by the spectrophotometer settings. Once the number and the approximate frequency of the different components are known, curve-fitting procedures can be applied to quantify the area of the different components of the amide envelope (much care must be taken then to prevent the appearance of artefacts due to the numerical treatment). It was only in 1986 that the first comprehensive study of a series of proteins of known structure has been reported by Byler and Susi. The agreement between the infrared-determined structure and the data obtained by analysis of X-ray diffraction was remarkable [6]. Since then, a large number of proteins have been studied according to similar protocols. All these studies were performed using solutions in H_2O or ^2H_2O [7–11]. In the present paper we demonstrate that the secondary structure of proteins can be determined on thin hydrated films of proteins by attenuated total reflection (ATR) spectroscopy. There are several advantages to this method: it requires small amount of materials (typically 10 μg), it does not require the knowledge of the protein concentration, it is not disturbed by highly turbid samples, such as large membrane fragments or precipitates, and finally, it allows the determination of the orientation of the secondary structures for membrane proteins with respect to the bilayer plane. The suitability of this method for membrane proteins has prompted us to add to the study of soluble proteins whose structure has been well characterized by X-ray crystallography, some of the best-characterized membrane proteins reconstituted in their bilayer environment, even though no high-resolution X-ray structures are available to day. We also introduce an automated treatment of the data which prevents human choice of the input parameters used for the curve fitting. We believe that only such an approach can be used comparatively by different investigators. Finally, we demonstrate that the protein concentration can be simultaneously determined for samples containing from 1–200 μg protein by using a phospholipid as an internal standard. In turn, for membrane samples the lipid/protein ratio can be easily and quickly estimated, a process which is often hampered by the presence of lipid when other techniques are used.

Correspondence to E. Goormaghtigh, Université Libre de Bruxelles, Campus Plaine CP 206/2, B-1050 Bruxelles, Belgium

Abbreviations. ATR, attenuated total reflection; FTIR, Fourier-transform infrared spectroscopy; $Myr_2GroPCho$, dimyristoylphosphatidylcholine; OcGlc, octyl-glucopyranoside; FWHH, full width at half height.

MATERIALS AND METHODS

Proteins and lipids

Most proteins were purchased from Sigma: bacteriorhodopsin from *Halobacterium halobium* (B3636), carbonic anhydrase from bovine erythrocytes (C7500), concanavalin A type IV (C2010), α-chymotrypsin from bovine pancreas (C2020), α-chymotrypsinogen from bovine pancreas (C4879), cytochrome *c* from horse heart (C2506), elastase from bovine pancreas (E0127), glycophorin from red blood cells (G9511), lysozyme from chicken egg white (L6876), myoglobin from sperm whale skeletal muscle (M0380), ribonuclease A from bovine pancreas (R5500), ribonuclease S from bovine pancreas (R6000), trypsin from porcine pancreas (T0134), trypsinogen from bovine pancreas (T1143) and trypsin inhibitor from soybean (T9003). Papain was a gift of Dr Y. Loose (Université Libre de Bruxelles) and porin was kindly supplied by Dr Rosenbusch (Biozentrum, Basel). L-α-Dimyristoylphosphatidylcholine ($Myr_2GroPCho$) came from Sigma. Reagents were all of the highest purity grade; water was triple-distilled and glass tubes were washed with concentrated sulfuric acid containing potassium dichromate. Octylglucopyranosides (OcGlc) was a Sigma reagent.

Membrane protein reconstitution

Glycophorin. 250 μg glycophorin A was solubilized in 500 μl 20 mg/ml OcGlc in 10 mM Tris, pH 7.5. 2.5 mg $Myr_2GroPCho$ was dissolved in $CHCl_3$. The lipid solution was then dried under a nitrogen stream to form a thin film on the glass tube wall. Residual traces of the organic solvent were further removed by placing the film under vacuum overnight. The lipid film was then dissolved in the glycophorin/OcGlc solution and the mixture was dialysed for 36 h at 4 °C against 10 mM Tris/Cl, pH 7.5 [12]. The vesicles were then run on a Sepharose CL-4B (Pharmacia) column equilibrated with H_2O.

Porin. 300 μg porin was dissolved in 20 mM phosphate buffer, pH 6.5, containing 1% (by vol.) octyloligooxyethylene, 150 mM NaCl and 3 mM NaN_3. This was added to a 300-μg $Myr_2GroPCho$ film (prepared as described above for glycophorin) dissolved in 20 mM Hepes, pH 7, containing 2% (by vol.) OcGlc, 10 mM $MgCl_2$, 0.1 M NaCl, 0.2 mM EDTA, 0.2 mM dithiothreitol and 3 mM NaN_3 [13]. The mixture was dialysed for 36 h at 4 °C against 2 mM Hepes, pH 7.5.

Bacteriorhodopsin. 700 μg bacteriorhodopsin was dissolved in 150 μl 20 mM Mes, pH 6.0, containing 2% (by vol.) OcGlc, 0.15 M KCl and 3 mM NaN_3 [14]. This mixture was then added to 2.8 mg $Myr_2GroPCho$ in suspension in the same buffer. The solution was then dialyzed for 36 h at 4 °C against 20 mM Mes, pH 6.0, and finally against water.

Infrared spectroscopy

For general information about internal reflection infrared spectroscopy, see Harrick [15]. Details about the application of infrared ATR spectroscopy to membrane research were reviewed by Fringeli and Günthard [16]. ATR Fourier-transform infrared spectra (FTIR) were obtained on a Perkin Elmer 1720X FTIR spectrophotometer equipped with a liquid nitrogen cooled mercury-cadmium-telluride detector at a resolution of 2 cm^{-1}. 1024 scans were averaged. Every four scans, reference spectra of a clean germanium plate were automatically recorded and rationed against the recently run sample spectra by an automatic sample shuttle accessory. The spectrophotometer was continuously purged with dry air. For polarization experiments, a Perkin Elmer silver bromide polarizer was placed before the sample and the reference plate. The internal reflection element was a germanium ATR plate (50 × 20 × 2 mm, Harrick EJ2121) with an aperture angle of 45°, yielding 25 internal reflections. Spectra were recorded at a nominal resolution of 2 cm^{-1}.

Sample preparation for infrared spectroscopy

Germanium internal reflection elements were washed first with a laboratory detergent, then with methanol and finally with chloroform. Prior to use, they were placed for 3 min in a plasma cleaner (Harrick), a step which is essential for making the surface of the germanium clean and wettable.

Soluble proteins were dissolved in H_2O at a concentration of 2 mg/ml. 50 μl (100 μg) was dried on the surface of the germanium internal reflection element under N_2.

Membrane proteins were reconstituted in $Myr_2GroPCho$ liposomes, oriented multilayers were obtained as described by Fringeli and Günthard [17] by slowly evaporating 40 – 100 μl of the sample on one side of the ATR plate under N_2 at room temperature. The efficiency of the procedure was checked by measuring the dichroic ratio (see below) for the $\gamma_w(CH_2)$ vibration at 1200 cm^{-1}. A dichroic ratio higher than three indicated that the average tilt between the hydrocarbon chain and relative to the germanium surface, determined as described below, was smaller than 25°. Other information about oriented multilayer formation has been described elsewhere [17 – 21].

Samples for protein concentration determination were prepared by adding the desired amount of protein in 50 μl to a $Myr_2GroPCho$ film obtained by evaporating under nitrogen, then under vacuum overnight, 100 μl chloroform containing 100 μg $Myr_2GroPCho$. The sample was then dried on the germanium plate as described for the reconstituted membrane proteins.

The ATR plate was then sealed in a universal sample holder (Perkin-Elmer 186-0354) and hydrated by flushing ^2H_2O-saturated N_2 (room temperature) for 4 h. During this period of time, only the readily accessible peptide bonds are exchanged. Importantly, the random structure (see below) shifts from about 1655 cm^{-1} to about 1640 cm^{-1} upon H/^{2}H exchange, allowing differentiation of the α-helix from the random structure [22, 23]. Protons belonging to the peptide bonds of ordered structures as α-helices, and especially transmembrane α-helices are not expected to exchange significantly under our experimental conditions [24]. To avoid recording spectra of material not included in the cavity of the universal sample holder, which is atmosphere controlled, only a 10-mm window was left open on the middle of the aperture of the ATR plate; the two side bonds were masked by a thick teflon sheet.

Secondary structure determination

The main features of the procedure described by Byler and Susi [6] were followed with two major modifications. First, the procedure was entirely automated so that the input parameters for curve fitting were determined by our program. Second, in order to avoid possible artefacts arising from the deconvolution step and influencing the proportions of the different secondary structures, the final curve fitting was carried out on a spectrum obtained with very little deconvolution (see below).

The secondary structure of the proteins was determined from the shape of amide I′. Using synthetic polypeptides, e.g. polylysine [1, 25], as well as normal coordinate analysis [26], it was shown that this band was conformation sensitive, the α-helical structure having a maximum near 1655 cm^{-1} and the β-sheet structure having a maximum near 1630 cm^{-1}. Besides its important conformational sensitivity, the amide I band was located in a region of the infrared spectrum often free of other bands (most phospholipids and even complex mixtures such as asolectin do not absorb significantly in this region) [27], allowing the study of membrane proteins. Moreover, it was made out of 80% pure ν(C=O) vibration [28]. It was therefore intrinsically simpler that amide II and was more suitable for orientation measurements. For these reasons, we have focused our attention on the analysis of the shape of amide I′ in the rest of this paper. The strong overlap of the different components of the amide I′ arising from the different secondary structures usually resulted in a broad, featureless envelope. Attempting a curve fitting on such a band, was meaningless (unknown number of bands, frequencies, etc). As a first step, we therefore used Fourier self-deconvolution using a Lorentzian line shape [full width at half height (FWHH) = 30 cm^{-1}] and a Gaussian line shape for the apodization. This procedure has been detailed elsewhere [29]. Prior to curve fitting, a straight base line passing through the ordinates at 1700 cm^{-1} and 1600 cm^{-1} was subtracted. This seemed to be a reasonable choice since no significant protein absorption occurred at those wavelengths. The spectrum arising from the lipid part of the system (when present) was found to be completely flat between 1700 cm^{-1} and 1600 cm^{-1} and was therefore not subtracted. The base line was modified again by the least-squares curve-fitting program which allows for a horizontal baseline to be adjusted as an additional parameter to obtain the best fit. The spectrum between 1700 cm^{-1} and 1600 cm^{-1} was also normalized between absorbances of 0 and 1. A first least-squares iterative curve fitting was then performed with Lorentzian bands [30]. The input parameters for this first curve fitting were chosen by our program as follows: only a limited number of Lorentzian bands of given frequency were allowed: 1695 cm^{-1}; 1683 cm^{-1}; 1678 cm^{-1}; 1672 cm^{-1}; 1664 cm^{-1}; 1657 cm^{-1}; 1648 cm^{-1}; 1640 cm^{-1}; 1632 cm^{-1}; 1624 cm^{-1}. These frequencies were chosen because they often appear in deconvoluted spectra of proteins. The intensity was chosen to be a fraction x of the intensity of the spectrum at this frequency. x and the width of the Lorentzian $\Delta\nu$ are a function of the resolution enhancement factor, K [29] defined as the ratio of the FWHH $\Delta\nu$ of the deconvoluting Lorentzian to the FWHH of the Gaussian used for apodization [29]. For $K > 2.2$, $x = 0.9$, $\Delta\nu = 4$ cm^{-1}; for $1.8 < K < 2.2$, $x = 0.8$, $\Delta\nu = 6$ cm^{-1}; for $K = 1$, $x = 0.6$, $\Delta\nu = 10$ cm^{-1}. We must stress here that the narrowing effect of the Fourier self-deconvolution on a given band can be correctly described by factor K only if the line shape to be used for the deconvolution is known exactly, which is virtually never the case in infrared spectroscopy of proteins [31]. If the spectral intensity of the normalized amide I′ band is less than 0.25 for the frequency of a band, the band is rejected. This first curve fitting was carried out on spectra deconvoluted with $K > 2-2.8$. Under such conditions, the amide I′ band presents well-defined maxima and the fitting was carried out. In the next step, we use the bands resulting from this curve fitting as input parameters for a fitting on the spectrum deconvoluted with $K = 1$. Only the value of $\Delta\nu$ was readjusted by the program as explained above. The resulting fitting was analyzed as follows: each band was assigned to a secondary structure according to the frequency of its maximum. The areas of all bands assigned to a given secondary structure were then summed up and divided by the total area. The number, so obtained, was taken to be the proportion of the polypeptide chain in that conformation. We must stress that we made here the assumption that the absorption coefficients were equal for all the secondary structures, this assumption has still to be demonstrated. The frequency limits used were empirically determined (see [27]) and were as follows: 1662 – 1645 cm^{-1}, α-helix; 1689 – 1682 cm^{-1} and 1637 – 1613 cm^{-1}, β-sheet; 1644.5 – 1637 cm^{-1}, random; 1682 – 1662.5 cm^{-1}, β-turns.

Orientation determination

In an α-helix, the main transition dipole moment [ν(C=O)] lay almost parallel to the helix axis while in an antiparallel β-sheet the polarisation was opposite i.e. predominantly perpendicular to the fiber axis [28]. It was therefore possible to determine the mean orientation of the α-helix and β-sheet structures from the orientation of the peptide bond C=O group. When that information was desired, additional spectra were recorded with parallel (0°) and perpendicular (90°) polarized incident light, with respect to a normal to the ATR plate. Polarization was expressed as the dichroic ratio $R_{atr} = A^{90°}/A^{0°}$. The mean angle between the C=O bond and a normal to the ATR plate surface was then calculated from R_{atr} according to Fringeli and Günthard [16]. For the α-helix orientation, a 27° deviation between the α-helix axis and the C=O dipole moment, described by Rothschild and Clark [32], was taken into account by introducing an order parameter $S_{C=O} = (3\cos^2 27° - 1)/2$ so that $S_{helix} = S_{measured}/S_{C=O}$. The angle between the helix axis and the normal to the bilayer we arrive at was therefore a minimum estimate and an orientation of the helix axis closer to this normal would result from considering other sources of disorder such as an imperfect parallelism between the bilayers and the germanium crystal surface.

Protein concentration assay

Spectra were recorded as described but before the deuteration step. The area of the lipid ν(C=O) band near 1736 cm^{-1} was evaluated after drawing a straight base line between 1770 cm^{-1} and 1700 cm^{-1}. These two limits were then slightly modified (within 15 cm^{-1}) in order to be located at a frequency corresponding to a minimum of the spectrum. Similarly, the area of amide I was measured between about 1700 cm^{-1} and 1600 cm^{-1}.

RESULTS

The infrared spectrum of three deuterated proteins characterized by a high α-helix content (myoglobin), an equal proportion of α-helic and β-sheets (papain) and a high β-sheet content (α-chymotrypsin) appear in Fig. 1. The amide I′ maximum appears at 1650 cm^{-1} for myoglobin, 1636 cm^{-1} for α-chymotrypsin and as a doublet for papain. The shift of amide II (1550 cm^{-1}) towards amide II′ near 1450 cm^{-1} upon H/^{2}H exchange is essentially complete here, allowing the ring vibration of tyrosine at 1515 cm^{-1} to appear clearly. Fig. 2 represents, in a similar way three membrane proteins reconstituted in a $Myr_2GroPCho$ bilayer as described in Materials and Methods. Bacteriorhodopsin is characterized by a high α-helix content, porin by a high β-sheet content, and glycophorin by a mixture of both structures. It is clear from the comparison

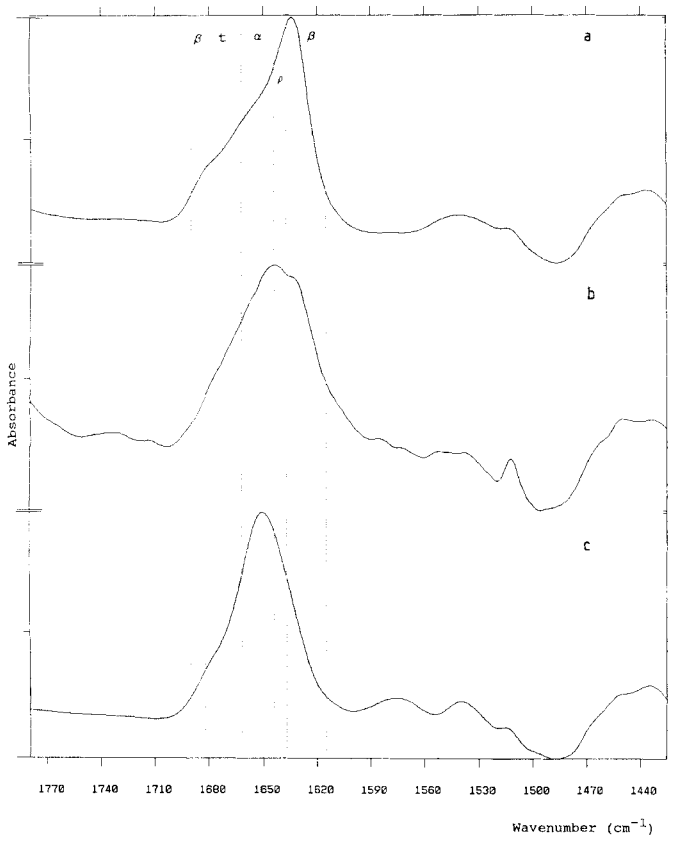

Fig. 1. *Infrared-ATR spectrum of deuterated films of three soluble proteins.* (a) α-Chymotrypsin; (b) papain; (c) myoglobin. The dotted lines limit the region assigned to the different secondary structures defined in Materials and Methods: β, β sheet; α, α helix, t, β turns and ϱ, random. Amide I′ of each spectrum has been rescaled to the same amplitude

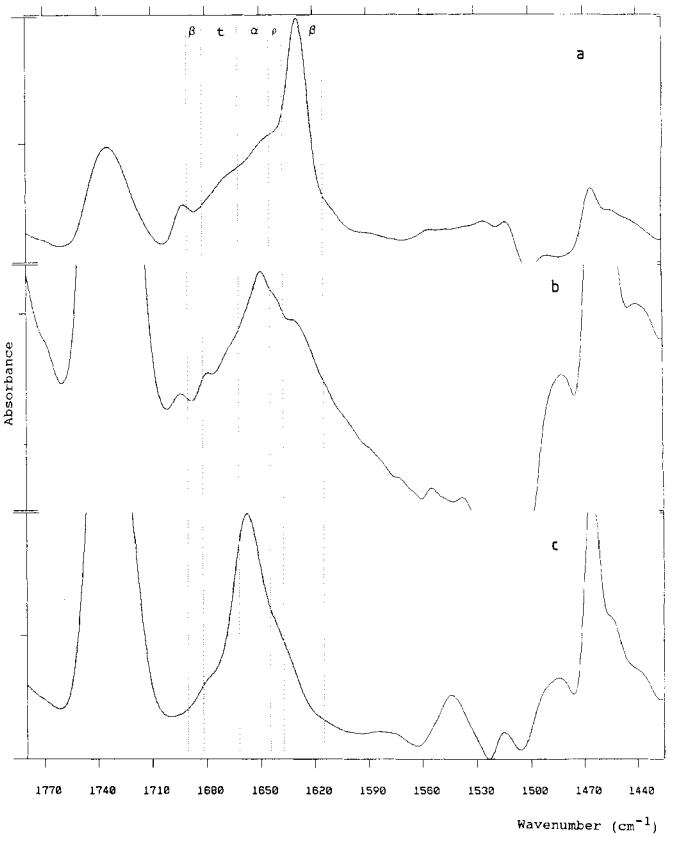

Fig. 2. *Infrared-ATR spectrum of deuterated films of three membrane proteins reconstituted in a $Myr_2GroPCho$ bilayer as described in Materials and Methods.* (a) Porin; (b) glycophorin; (c) bacteriorhodopsin. The dotted lines limit the region assigned to the different secondary structures (see Fig. 1). Amide I′ of each spectrum has been rescaled to the same amplitude

of Figs 1 and 2 that membrane proteins have an infrared spectrum in the amide I′ region similar to that of soluble proteins of similar secondary structure. The definite influence of the secondary structure on the shape of amide I′ appears even more clearly in Fig. 3A for a series of proteins characterized by high β-sheet content with no α-helix (Fig. 3A, a) to almost all α-helix (Fig. 3A, h). Fourier self-deconvolution (Fig. 3B) allows the resolution of some of the features of the broad bands displayed in Fig. 3A. The way the secondary structure of the protein is quantified is presented in Fig. 4. First, a set of automatically determined input parameters (see Materials and Methods) are used for an iterative curve fitting on a Fourier self-deconvoluted spectrum, similar to those presented in Fig. 3B. The bands resulting from the fitting (Fig. 4A) are then reinjected with the modifications described in Materials and Methods as input parameters for a new curve on a much less deconvoluted spectrum (Fig. 4B and C). As observed in Fig. 4, the position of the various components once established by the first curve fitting remains fairly constant when the new curve fitting is applied to less deconvoluted spectra. Moreover, if the secondary structure is evaluated at each step presented in Fig. 4, it appears that it remains quite constant. Those features are characteristic of the data treatment presented in this paper. The final fitting results for myoglobin (mainly α-helix) and α-chymotrypsin (mainly β-sheet) appear in Fig. 5. Results obtained for more soluble and membrane proteins are compared to the X-ray data analysis or, if not available, to other types of secondary structure determination in Table 1. Table 2 reports the frequency of the components determined by the curve fitting for the same set of proteins.

Results of polarization measurements appear for the α-helix-rich membrane protein bacteriorhodopsin, and for the β-sheet-rich membrane protein porin in Fig. 6. Spectra were recorded with two polarizations of the incident light, called here 90° and 0°. 0° is polarized in the plane of the germanium plate and 90° is perpendicular to 0° polarisation. The strong 90° polarisation of the phospholipid $\gamma_w(CH_2)$ at 1200 cm^{-1} and the 0° polarisation of the phospholipid $\delta(CH_2)$ at 1468 cm^{-1} [16] demonstrate that the phospholipid acyl chains are oriented almost perpendicular to the germanium plate, i.e. the bilayer lies parallel to the germanium surface. These two peaks appear on the dichroism spectra obtained by subtracting the 0° spectrum from the 90° spectrum, respectively, as a positive and negative deviation from the baseline (Fig. 6). While the lipid $\nu(C=O)$ at 1736 cm^{-1} is only weakly polarized, the amide I band associated with the porin β-sheet at 1629 cm^{-1} and with the bacteriorhodopsin α-helices at 1661 cm^{-1} are both strongly 90° polarized, indicating that the C=O double bonds of the peptide bond are oriented preferentially perpendicular to the membrane plane.

Evaluation of the protein concentration was obtained by mixing a protein solution with a phospholipid suspension as an internal standard as described in Materials and Methods. Fig. 7 reports the spectra of 100 μg $Myr_2GroPCho$ mixed with 1.78 μg lysozyme (Fig. 7a), 17.8 μg lysozyme (Fig. 7b)

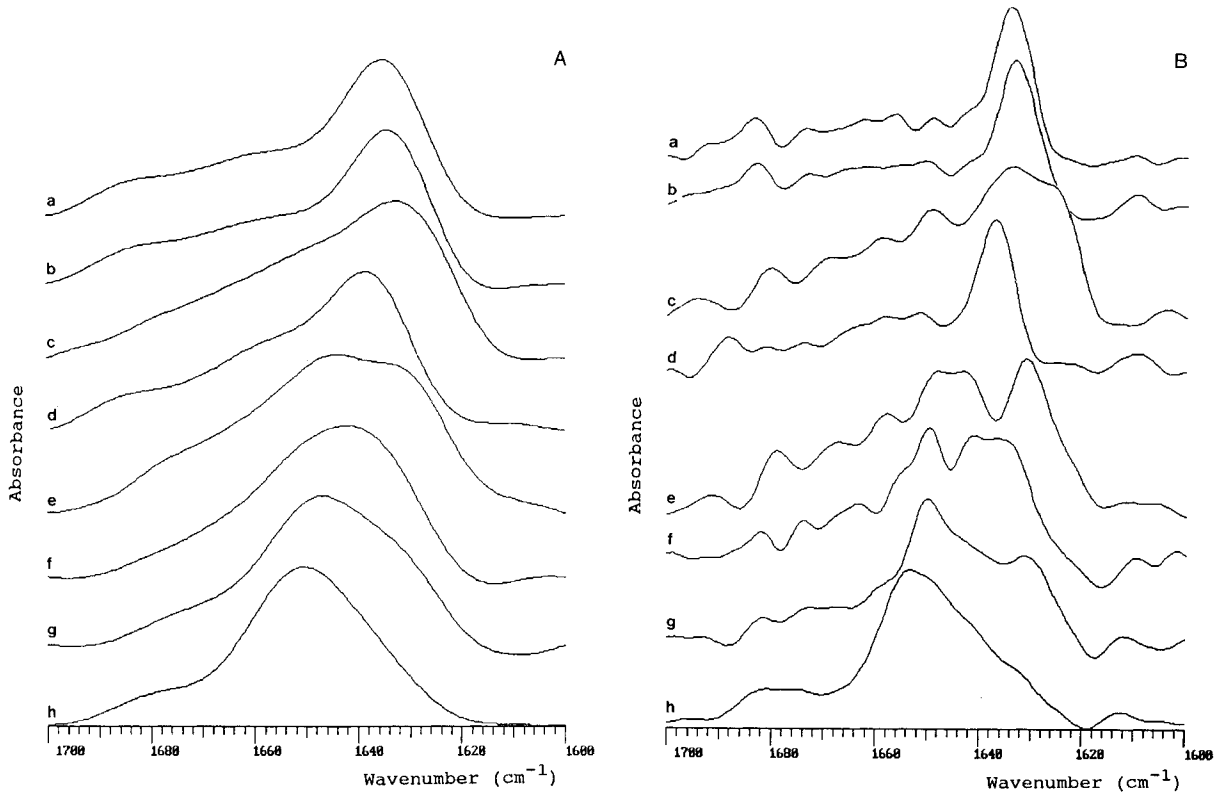

Fig. 3. *Infrared-ATR spectrum in the amide I′ region of deuterated films of a series of soluble proteins rich in β-sheet with small amount of α-helic (top) to almost pure α-helix (bottom).* (A) α-chymotrypsin (a); trypsin (b); carbonic anhydrase (c); ribonuclease A (d); papain (e); lysozyme (f); cytochrome *c* (g); myoglobin (h). (B) As in (A), but after Fourier self-deconvolution with a resolution enhancement factor of $K = 2$ [29]. Amide I′ of each spectrum has been rescaled to the same amplitude and is drawn with an offset

and 100 μg lysozyme (Fig. 7c). The ν(C=O) lipid band at 1736 cm^{-1} is virtually absent for the pure protein and no absorption occurs in the amide I region between 1700 cm^{-1} and 1600 cm^{-1} for the pure lipid (not shown). The ratio of the integrated intensities of the amide I band to the lipid ν(C=O) was therefore taken as a measure of the protein/lipid ratio. The relation between these two quantities appears in Fig. 8 for lysozyme. Clearly, an accurate determination of the protein concentration can be obtained for a wide range of protein concentration. When an α-helix-rich protein such as myoglobin, or a β-sheet-rich protein such as α-chymotrypsin, are used, similar relations were obtained (not shown).

DISCUSSION

The procedure described to evaluate the secondary structure of proteins yields an estimation of the α-helix and β-sheet content with a standard deviation of 8.7% with respect to the X-ray structure, in contrast to the procedure described by Byler and Susi which yielded a deviation smaller than 2.5% [6]. In the latter case, such an achievement was made possible by manual introduction of the input parameters for the curve fitting and by letting the least-squares fitting program adjust only one parameter at a time. In our hands, such a practice yields indeed smaller deviations for a trained investigator, but we consider that the new, completely automatic procedure described in the present paper for choosing the input parameters of the curve fitting is an important step in the way of making this technique more objective and more accessible to all investigators. Theoretical obstacles limit the interpretation of the result of the curve fitting.

The Fourier self-deconvolution technique used here has the property of enhancing selected frequencies of the spectrum. In the absence of an accurate description of the function necessary to deconvolute the spectrum, the details so resolved should be considered to be without physical meaning. The so-called resolution enhancement factor, K, [29] also loses any physical meaning when the deconvoluting function is not correctly defined [31]. The effect of the deconvolution parameters on the shape of the deconvoluted spectrum is illustrated in Fig. 9 where the spectrum of papain has been analyzed as described in Fig. 4 but for a deconvolution performed with a FWHH of the deconvoluting Lorentzian of 20 cm^{-1} and 40 cm^{-1} (instead of 30 cm^{-1} in Fig. 4). The reasons for the differences between the different deconvolution parameters appear most clearly when the deconvolution-apodization function shape in the transformed domain $DA(x)$ is compared for the various FWHH used (Fig. 10). This shape is defines by [31]

$$DA(x) = \sqrt{\ln 2}\exp(2\pi\sigma_l|x| - \pi^2\sigma^2{}_g x^2/\ln 2)$$

where $\sigma_l = {}^1/_2$ FWHH of the deconvoluting Lorentzian and $\sigma_g = {}^1/_2$ FWHH of the apodization Gaussian. x is expressed in cm. The maximum of the function occurs at [31]

$$x_{max} = \frac{\ln 2\,\sigma_l}{\pi\sigma^2{}_g}.$$

Clearly Fig. 10 indicates that the frequencies most enhanced are different for each value of K as the FWHH varies and explains why the spectrum deconvoluted with FWHH = 20 cm^{-1} and $K = 1.0$ resembles the spectrum deconvoluted with FWHH = 40 cm^{-1} and $K = 1.8$ in Fig. 9. Since, until

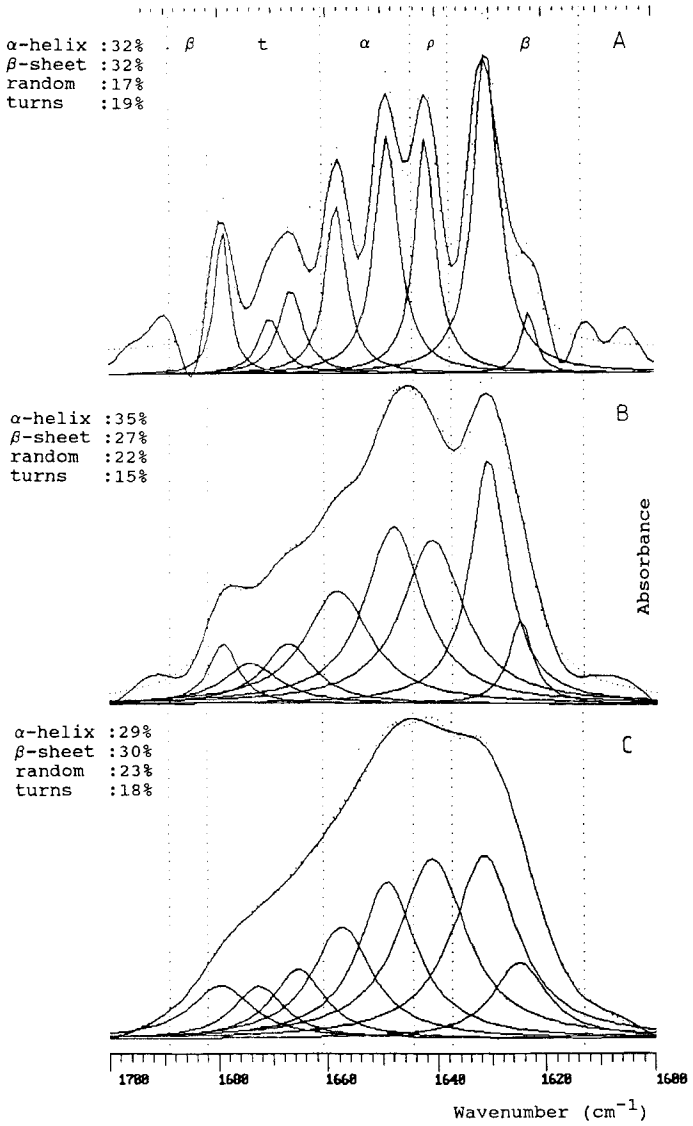

Fig. 4. *Secondary structure determination of papain.* The papain film has been deuterated as described in Materials and Methods. The figure represents the infrared-ATR spectrum of the film in the amide I region at three stages of the deconvolution process: $K = 1$ (C), $K = 1.8$ (B) and $K = 2.4$ (A). The intensity, width and frequency of the Lorentzian band used for the curve fitting were chosen by the program on the basis of the shape of the most deconvoluted spectrum (A). An iterative least-squares curve-fitting program then adjusted these input parameters and a base line to produce fitted bands which appear under spectrum (A). These adjusted parameters were then reported as input parameters to fit spectrum (B) and spectrum (C) after modification of their width according to the protocol described in Materials and Methods. The result of the fitting appears under curve (B) and (C). The vertical dotted lines define the region of the spectrum assigned to the different secondary structures as described in Fig. 1. The sum of the components is represented by the dotted spectrum. Amide I′ of each spectrum has been rescaled to the same amplitude

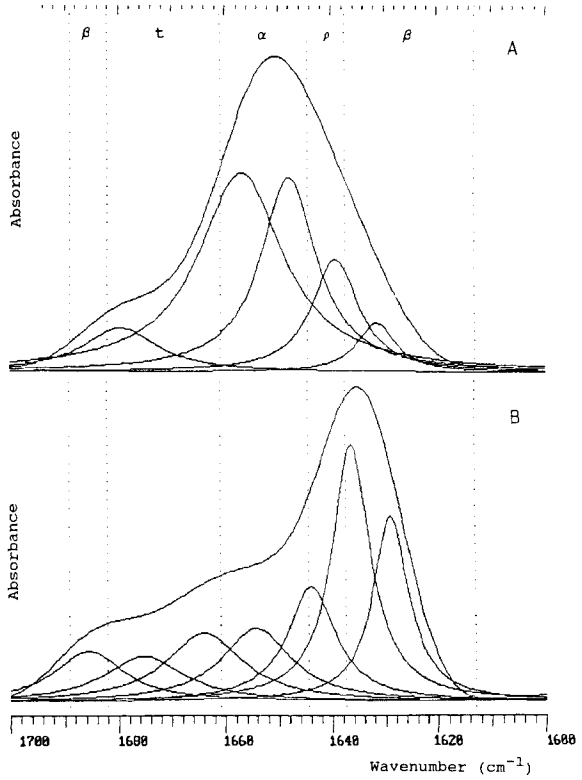

Fig. 5. *Results of the Fourier self-deconvolution curve-fitting procedure as described in Fig. 4 for an α-helix-rich protein, myoglobin (A), and for a β-sheet-rich protein, α-chymotrypsin (B).* The vertical dotted lines have the same meaning as in Fig. 1. Amide I′ of both spectra has been rescaled to the same amplitude

now, there has been no satisfactory description of the shape of the function which should be used to remove specifically the broadening of the components of amide I′ brought from different origins in the liquid or solid state, Fourier self-deconvolution must therefore be considered as a trick which allows a unique curve fitting to be performed for a given spectrum and for given self-deconvolution parameters. Yet, as demonstrated in Figs 4 and 9, the procedure described here ultimately yields similar secondary structure estimations for the different deconvolutions. Other potential artifacts of Fourier self-deconvolution, such as these coming from the transformation of an originally random noise into a spectrum similar to a sample signal [31] or the enhancement of weak bands arising from unbalanced atmospheric water [39] have been discussed elsewhere. In conclusion, in the present state of our knowledge, Fourier self-deconvolution is useful for the curve-fitting step but in most cases one should not attempt to assign the various components of amide I′, which appear for high values of K, to well-defined physical structures. In some instances discussed below, evidence indicates that it is possible to distinguish subcomponents among various types of secondary structures, but these indications are then substantiated by other data such as polarization features.

The analysis of the data presented here, to evaluate the secondary structure of proteins, is based on several hypotheses: the integrated absorption coefficients are supposed to be equal for all the structures, the contribution of the side chains of the amino acid residues to the amide I band is supposed to be negligible, no overlapping of the different component assigned to each structure occurs, and finally, the formation of a thin hydrated film does not modify the secondary structure. The results of the analysis reported in Table 1 indicate that these assumptions are reasonable. Indeed, a correct assessment of the secondary structure, to within a few percent, was achieved for all the proteins tested. It must be stressed here that the secondary structure computed from a single three-dimensional structure obtained by X-ray diffraction may show considerable variations according to the criteria used to recognize the different secondary structures. Here

Table 1. *Secondary structure of soluble and membrane proteins estimated by infrared (IR) spectroscopy and by other methods*
For soluble proteins, X-ray data analysis are from Levitt and Greer [33], see [34–36] for bacteriorhodopsin, [37] for glycophorin and [38] for porin. For the soluble proteins, the mean deviation was ±1.1% with a standard deviation σ of ±8.7% (n = 28)

Protein		Secondary structure			
		α-helix	β-sheet	random	β-turns
		%			
Cytochrome *c*	IR	40	16	18	25
	X-ray	49	10		
Lysozyme	IR	49	13	23	26
	X-ray	45	19		
Papain	IR	29	30	23	18
	X-ray	29	29		
Ribonuclease A	IR	28	38	16	20
	X-ray	22	46		
Ribonuclease S	IR	25	42	16	17
	X-ray	23	53		
Myoglobin	IR	68	7	14	10
	X-ray	87	0		
Carbonic anhydrase	IR	28	37	17	18
	X-ray	16	45		
α-Chymotrypsinogen	IR	11	47	12	30
	X-ray	11	46		
α-Chymotrypsin	IR	11	58	12	19
	X-ray	10	49		
Trypsin inhibition	IR	11	52	15	19
	X-ray	0	50		
Trypsinogen	IR	23	46	15	16
	X-ray	9	56		
Trypsin	IR	12	58	12	19
	X-ray	9	56		
Concavalin A	IR	20	54	15	10
	X-ray	2	60		
Elastase	IR	24	39	15	23
	X-ray	10	47		
Bacteriorhodopsin	IR	63	15	11	11
	IR, CD, electron diffraction	45–80			
Glycophorin	IR	32	24	25	19
	CD (in solution)	27	10		
Porin	IR	19	60	10	12
	Raman	9	54	13	24

we have consistently used the analysis performed by Levitt and Greer which uses hydrogen bonds, the inter-Cα distances and the inter-Cα torsion angles as a reference [33], but we do not know yet whether another set of criteria would yield secondary structures better related to infrared spectra. It is indeed an additional hypothesis that the criteria used by Levitt and Greer [33] match the structural elements which define the amide I′ band shape. In addition to the rather arbitrary splitting of amide I′ into well-resolved components by Fourier self-deconvolution discussed above, this remark bears upon the meaning which is to be given to each individual component determined during the course of the curve fitting. Experimental evidence indicates that, depending on the protein, the α-helix or the β-sheet component can be very broad [40] and split into several subcomponents. Theoretical work indicates for instance that the frequency of the α-helix depends on the length of the helix [41]. Moreover, the central and terminal regions of an α-helix could yield different spectra. Any distortion of the α-helix would also shift the frequency of the amide-I-associated band. Such distorsions have been recently described in protein crystals [42]. It therefore appears wiser to consider the individual components determined by the curve fitting as a mixture of many subcomponents with slightly different frequencies. More theoretical and experimental work is needed to clarify this point. However, the comparison of the frequencies of the component determined here and elsewhere for ribonucleases A and S [43] and for concanavalin A [44] points out a general similarity between the different analysis but also some differences. Splitting of the α-helix and the β-sheet component spontaneously occurs in the procedure described in this paper and can already yield important information for membrane proteins. For instance, a low-frequency

Table 2. *Frequency of the components resulting of the curve fitting of amide I' for the proteins tested in Table 1*
The rounded frequency of each component defined by a curve fitting similar those reported in Figs 4C and 5 is reported for each protein. The assignment of these components to a defined secondary structure is realised as explained in Materials and Methods and appears in the heading on top of each column. RMS, root mean square associated with the fitting

Protein	Wavenumber									RMS
	α-helix	α-helix	β-sheet	β-sheet	β-sheet	β-turn	β-turn	β-turn	random	
	cm^{-1}									%
Cytochrome *c*	1657	1649		1632	1626	1676	1675	1665	1640	2.7
Lysozyme	1654	1646		1630		1678	1670	1662	1638	3.7
Papain	1657	1649		1632	1625	1680	1673	1665	1641	0.7
Ribonuclease A	1657	1649	1686	1633	1622	1678	1671	1664	1641	0.8
Ribonuclease S	1656	1648	1685	1632	1623	1677	1670	1664	1640	0.4
Myoglobin	1657	1648		1632		1679			1640	1.5
Carbonic anhydrase	1657	1648	1688	1631	1624	1680	1673	1665	1639	2.0
α-Chymotrypsinogen	1653			1636	1628	1682	1670	1662	1644	2.3
α-Chymotrypsin	1654		1683	1636	1629		1673	1663	1644	2.3
Trypsin inhibitor	1655	1645	1685	1637	1630	1678	1670	1663	1643	1.9
Trypsinogen	1656	1648	1683	1631	1624		1672	1664	1643	0.4
Trypsin	1654		1683	1636	1628		1672	1663	1644	3.0
Concavalin A	1658	1648	1684	1631	1623		1672	1665	1638	2.7
Elastase	1657	1648	1688	1632	1621	1679	1671	1664	1639	0.4
Bacteriorhodopsin	1658	1651	1684	1632	1625	1673	1666		1642	3.8
Glycophorin	1656	1650	1689	1630	1624	1677	1665		1641	1.4
Porin	1658	1651	1683	1634		1678	1664		1642	0.2

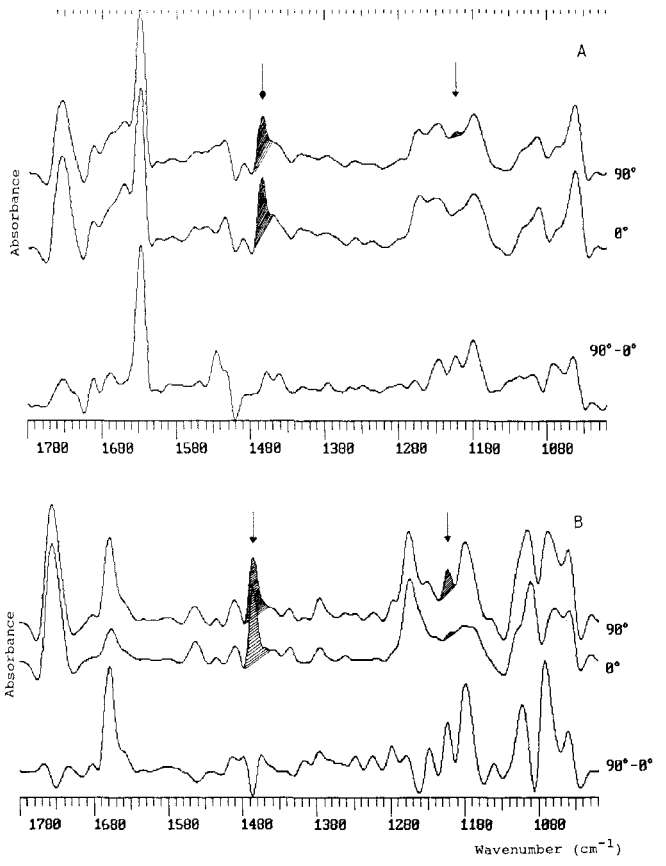

Fig. 6. *Polarized infrared-ATR spectra of deuterated films of porin (A) and bacteriorhodopsin (B) reconstituted in $Myr_2GroPCho$ bilayer as described in Materials and Methods.* Spectra were polarized at 90° and 0° (see text). Spectra have been deconvoluted with a resolution-enhancement factor, $K = 1.4$. The arrows indicate the phospholipid $\delta(CH_2)$ at 1468 cm^{-1} and the $\gamma_w(CH_2)$ at 1200 cm^{-1}. The dichroic spectrum (90−0°) has been rescaled

β-sheet component was found for the β-sheet structure associated to the surface of the lipid bilayer for diphtheria toxin fragment CB4 [27, 45] and for apoprotein B100 in human low-density lipoproteins [46] but not for most soluble proteins or for transmembrane oriented β-sheet such as in porin (this work). When this low-frequency β-sheet structure was found, polarisation measurements clearly indicate a specific orientation with respect to the membrane plane which does not exist for the usual β-sheet in the same proteins. The physical existence of two components revealed by Fourier self-deconvolution was then confirmed by polarisation measurements which indicate different orientations for the two components. Similarly, the α-helix of bacteriorhodopsin is located at an unusually high frequency (1661 cm^{-1}) which could characterize distortion of transmembrane helices in general [47]. Another example of such an agreement between Fourier self-deconvolution and dichroism measurements for resolving two components, has been reported for the complex poly-(Glu-Ala-Leu-Ala) peptide-$Myr_2GroPCho$ complex. The high-frequency component of the α-helix at 1658 cm^{-1} had a well-defined orientation with respect to the membrane plane, while the low-frequency component at 1648 cm^{-1} was not oriented [48]. The observation that at least in some instances membrane-associated structures have vibration frequencies unusual for soluble proteins is potentially crucial for the independent study of the structure and orientation of the polypeptide chain embedded in the lipid bilayer and the structure of the part of the protein protruding into the aqueous environment.

Dichroism measurements indicate that the most polarized component of the α-helix secondary structure of bacteriorhodopsin is located at 1662 cm^{-1} while it is located at 1629 cm^{-1} for the β-sheet component of porin (Fig. 6). These two maxima fit well with the observed absorption maxima of the infrared spectrum suggesting the presence of single types of β-sheet and α-helix with similar orientation throughout the protein, even though two components appear in the curve

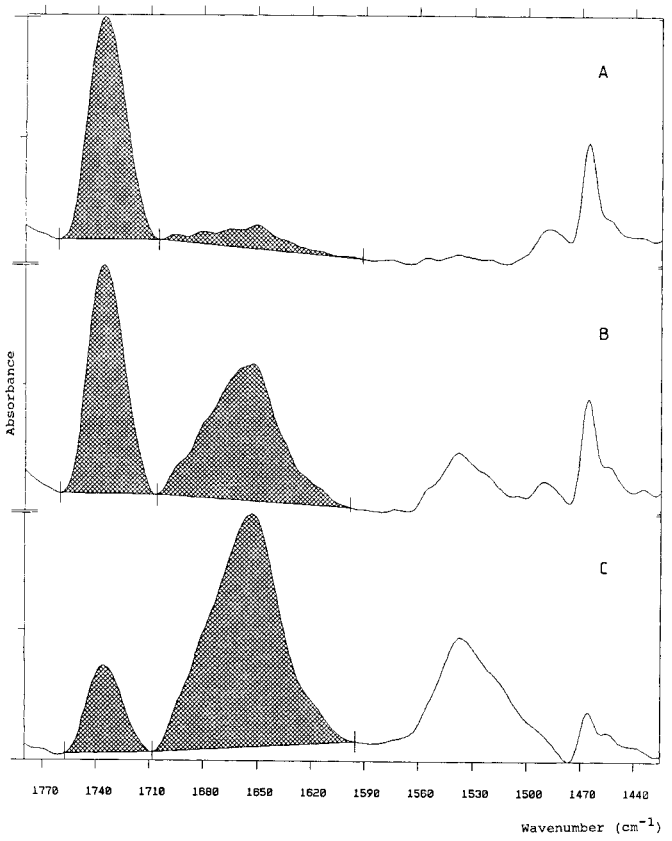

Fig. 7. *Infrared-ATR spectra of 100 μg $Myr_2GroPCho$ to which was added 1.78 μg lysozyme (A), 17.8 μg lysozyme (B) and 100 μg lysozyme (C).* The shaded area represents the lipid $\nu(C=O)$ integrated intensity and the unshaded area the protein amide I integrated intensity used to evaluate the lipid/protein ratio in the mixture

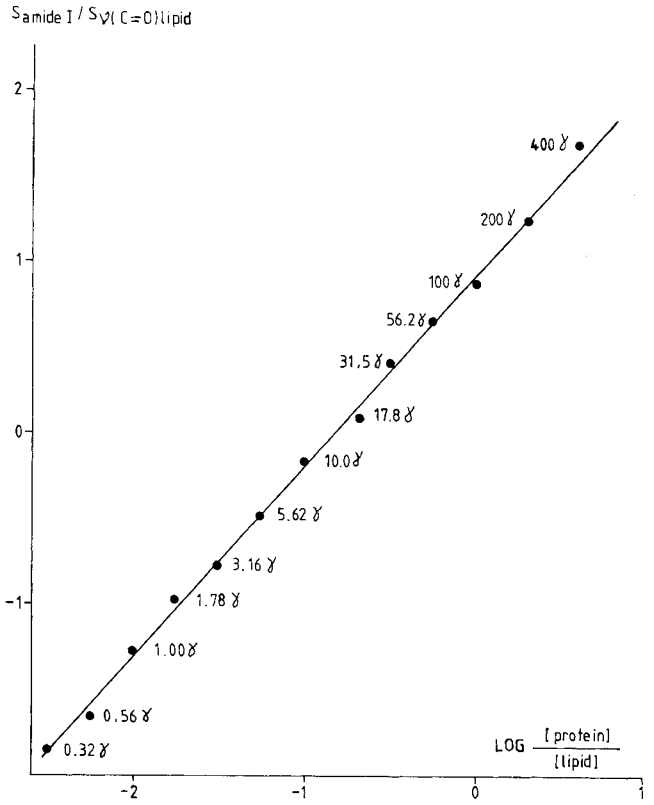

Fig. 8. *Calibration curve for lysozyme assay.* 100 μg $Myr_2GroPCho$ were mixed with the indicated amount of lysozyme. Log of the amide I area/lipid $\nu(C=O)$ area ratio (see Fig. 7) is reported as a function of log ([protein]/[lipid]) (by mass). The linear-regression correlation coefficient is 0.9992

fitting. The orientation of the α-helices of bacteriorhodopsin [49, 50] and of the β-sheet of porin [48, 49] has been reported previously and are in qualitative agreement with the present data. The orientation of the β-sheet component of the amide I′ band of porin resolved by Fourier self-deconvolution and curve fitting is characterized by a dichroic ratio $R = A^{90°}/A^{0°} = 1.8$, corresponding to a maximum tilt of the C=O bond of 35° with respect to the normal membrane. This value of the dichroic ratio is somewhat larger than the value determined by Nabedryk et al. [51] ($R = 1.1$, corresponding to a maximum tilt of 48°). One possible reason for this discrepancy lies in the fact that the method used here determines specifically the dichroic ratio of the β-sheet component, while in the former case the dichroism at 1634 cm^{-1} was used. Another possible explanation is that the ordering of the bilayer is higher on the germanium plate (this study) than on a $CaCl_2$ disc [51]. Both experiments however determine a mean oblique orientation of the C=O bond. The bearing of this orientation on the model of the pore has already been discussed [52]. In addition to previous reports, we have characterized here the orientation of the phospholipids of the bilayer, a point which is important to assess the overall membrane orientation on the germanium plate. The dichroic ratio of the $\gamma_w(CH_2)$ was calculated to be 3.5, corresponding to a maximum mean tilt of the all-*trans* hydrocarbon chains [16, 53] of $Myr_2GroPCho$ of 22° with respect to a normal to the germanium plate. The orientation of the α-helix component of the amide I′ band of bacteriorhodopsin resolved by Fourier self-deconvolution and curve fitting is characterized by a dichroic ratio $R = A^{90°}/A^{0°} = 3.3$, corresponding to a maximum tilt of the helix axis of 0° with respect to the membrane normal (see Materials and Methods). Again, the orientation of the all-*trans* hydrocarbon chains of the phospholipid is characterized by a high dichroic ratio ($R = 3.2$) corresponding to a maximum mean tilt of 23° with respect to the normal germanium surface. This mean helix orientation therefore fits the commonly accepted model in which the helices of bacteriorhodopsin are perpendicular to the membrane plane [54].

Experimental limitations of the technique are few: the buffer should not contain carboxylic acid such as in acetate or EDTA, and no carbonate which absorb in the amide I region. Most commonly used buffers such as Mes, Tris, Hepes, phosphate, etc., are quite acceptable. Among the phospholipids, the spectrum of phosphatidylserine interfers with secondary structure determination, but complex mixtures such as asolectin do not [45]. The total amount of buffer materials, including salts, should not largely exceed the mass of the sample to be analyzed. Indeed, in the presence of large amount of non-absorbing molecules, the intensity of the sample spectrum decreases in infrared-ATR spectroscopy and, in turn, the signal/noise ratio decreases in the amide I region. The use of ATR-infrared instead of classical transmission spectroscopy has been motivated by its high sensitivity and because it provides much more structural information when working with membrane samples, since it gives access to the orientation of several chemical bonds with respect to the membrane plane. A major question when working with ATR-infrared concerns the extent of protein secondary structure modification upon interaction with the germanium plate. This problem is satisfac-

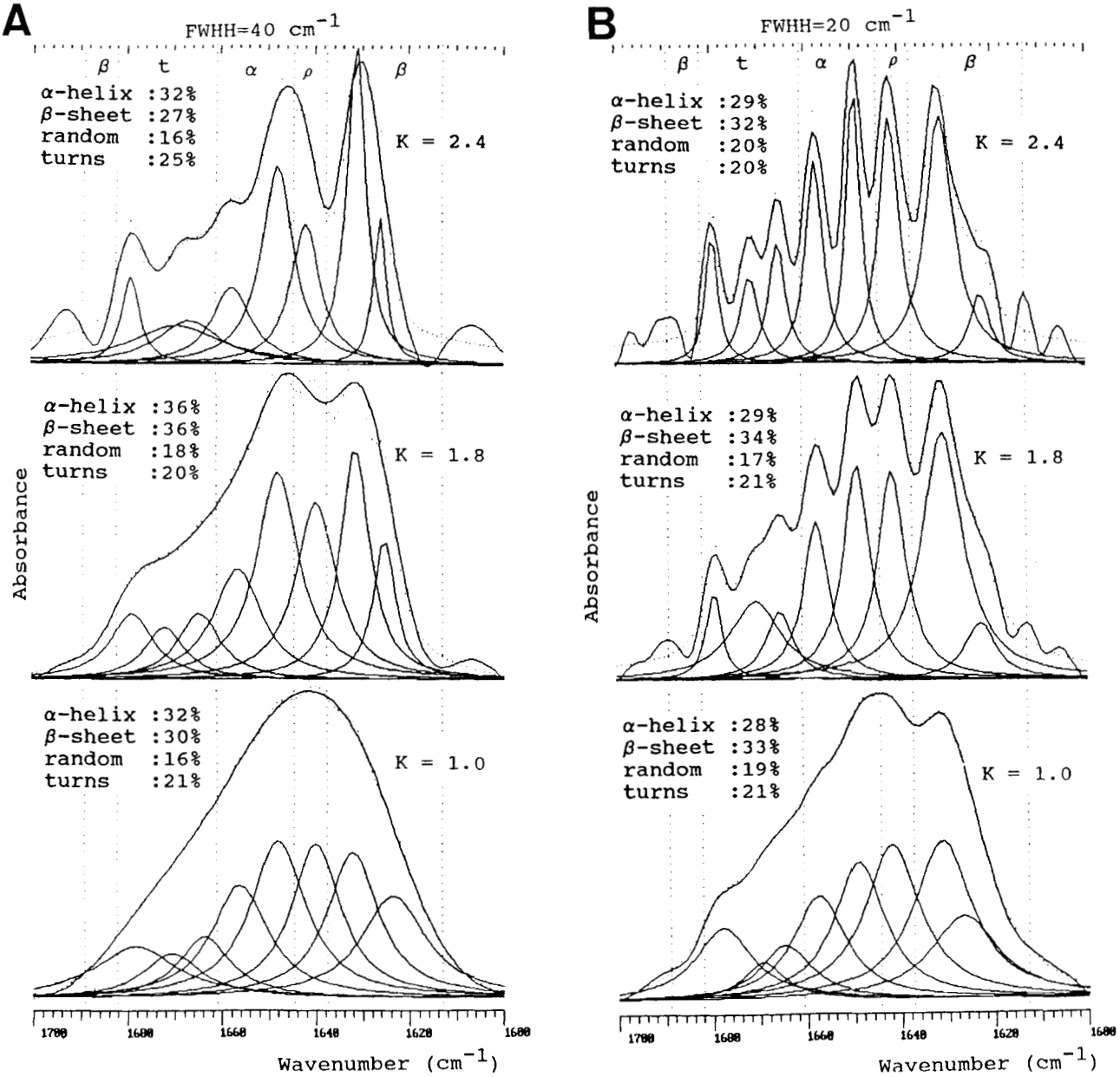

Fig. 9. *Secondary structure determination of papain performed on the sample described in Fig. 4 according to the same procedure except that the FWHH of the deconvoluting Lorentzian was 40 cm^{-1} (A) and 20 cm^{-1} (B) instead of 30 cm^{-1} on Fig. 4*

torily answered as follows. (a) When preparing a film of 100 μg protein, as described, on about 4 cm^2 of the ATR plate, the mean thickness of the film is 190 nm, considering an average relative density of 1.3 for the protein in the film. This is still a thin film with respect to the infrared wavelength (≈5 μm) and, according to the ATR theory [15], all its molecules will contribute about evenly to the spectrum, even though a small fraction of them is in direct contact with the ATR support. (b) If there were secondary structure changes for the fraction of protein in contact with the ATR support, these changes should be more visible when working with small amount of materials. However, in experiments not shown in which α-chymotrypsin, myoglobin and lysozyme were used, the spectra of films made up of only 1 μg protein were identical to those obtained with 100 μg protein, indicating that the hydrophilic surface of the germanium is not denaturating for the protein tested. Moreover, since in our experimental conditions only a small fraction of the protein molecules is in contact with the germanium surface, an effect of an interaction between the sample and the germanium plate would not threaten the validity of the analysis. The extent of the hydration of the protein in the sample hydrated film is more difficult to control; yet no difference appears between spectra recorded by the present method and by transmission in solution in some particular cases [46]. Moreover infrared spectra are well related to the structure determined by X-ray fraction data. The high concentration of protein in the hydrated film is probably similar to that found in protein crystals and may favour the comparison between the crystal structures obtained from X-ray diffraction and the structure of the protein in the hydrated films. Even small peptides such as the 21-amino-acid synthetic signal peptide of *PhoE*, on the germanium plate keeps the secondary structure it had in the solvent used for the preparation of the film [55]. The most critical step in the film preparation is

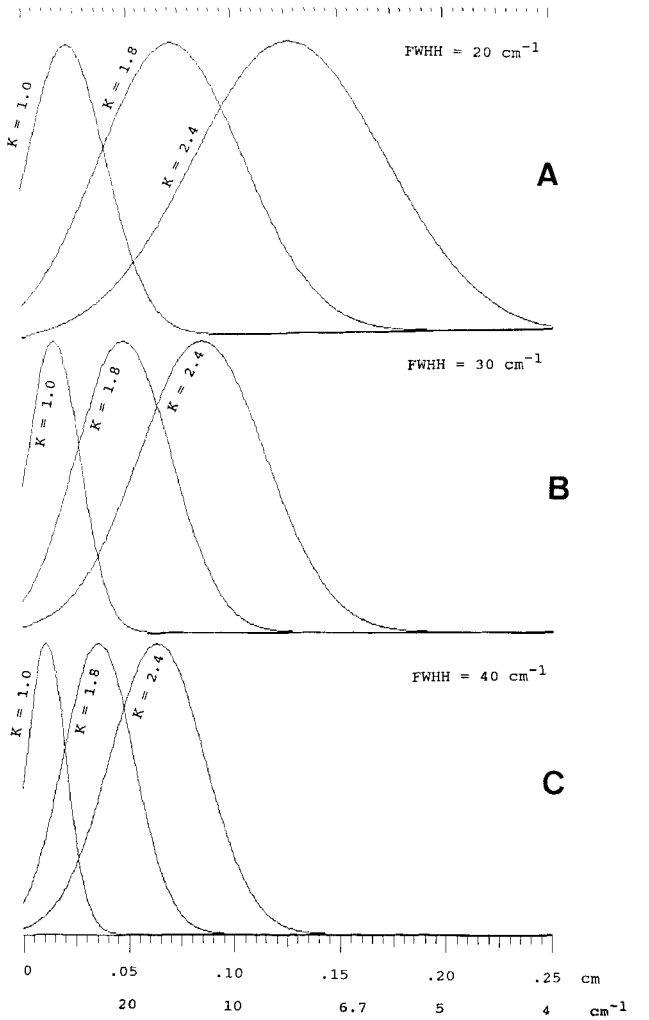

Fig. 10. *Shape of the deconvolution-adpodization function in the transformed fomain* DA(x) *(see text) for the three deconvolutions tested on the spectrum of papain and three values of the constant* K *used.* The value of 20 cm^{-1} (A) for the FWHH of the deconvoluting lorentzian was used in Fig. 9A. A value of 40 cm^{-1} (C) was used for the deconvolution reported in Fig. 9B and a value of 30 cm^{-1} (B) was used in the deconvolution reported in Fig. 4. Each curve has been rescaled to the same amplitude. The maximum amplitude of the curves is identical for a given value of K whatever the value of FWHH. It is 45 for $K = 2.4$, 7.9 for $K = 1.8$ and 1.7 for $K = 1.0$. The first abscissa scale is the transformed domain variable x while the second abscissa scale reports $\nu = 1/x$ in the frequency domain

encountered when the sample is dried before rehydration with ^2H_2O. This step is essential for the formation of oriented lipid multilayers [16, 56]. It must be noted that in the dry film the hydration water molecules are not removed, which explains why the secondary structure is usually not modified. Should a problem occur at this stage, the addition of a protectant such as trehalose [57, 58] would probably take care of it.

The estimation of protein concentration by infrared-ATR spectroscopy was shown to be very accurate when a calibration curve is available (correlation coefficient for linear regression = 0.9992). The protein concentration assay described is most useful for membrane-associated proteins and especially short peptides with atypical amino acid composition whose concentration is difficult to evaluate by the usual colorimetric methods (e.g. see [59]). Moreover, once the reconstitution of a protein in a lipid bilayer is achieved, the fraction of the protein which failed to include in the bilayer is usually eliminated. The infrared-ATR technique presented here provides a fast procedure able to accurately determine the efficiency of the reconstitution (lipid/protein ratio), a step which otherwise requires an assay for both the lipid and the protein. Moreover, the lipids present are likely to interfere with the colorimetric assay of the protein. Asolectin for instance yields a strong Lowry signal but is quite suitable for the infrared-ATR technique [45]. In the absence of a calibration curve, it is tempting to use an average calibration curve. Using the relation $S_{\text{amide I}}/S_{\nu(C=O)\text{ lipid}}$ = [Protein]/5 · [$Myr_2GroPCho$], where $S_{\text{amide I}}$ is the integrated area of amide I and $S_{\nu(C=O)\text{ lipid}}$ is the integrated area of the band at 1736 cm^{-1}, yields a correct estimate of the [Protein]/[$Myr_2GroPCho$] ratio (by mass) with a maximum deviation of 50% for all the proteins tested so far. A secondary structure analysis of the proteins and a knowledge of the specific extinction coefficients for the different secondary structures should help improve the latter situation in the future.

E.G. is an *Action de Recherche Concertée* (Belgium) fellow, V.C. is Senior Research Assistant for the National Fund for Scientific Research (Belgium). This work was supported in part by the *Banque Nationale de Belgique*, the National Fund for Scientific Research and the *Caisse Générale d'Epargne et de Retraite* (Belgium). We also thank the Commission of the European Community (contract SC 100195) for its financial support.

REFERENCES

1. Susi, H., Timasheff, S. N. & Stevens, L. (1967) *J. Biol. Chem. 242*, 5460–5466.
2. Suzuki, E. (1967) *Spectrochim. Acta 23A*, 2303–2308.
3. Talsky, G., Mayring, L. & Kreuzer, H. (1978) *Angew. Chem. Int. Ed. Engl. 17*, 785–799.
4. Kauppinen, J. K., Moffat, D. J., Mantsch, H. H. & Cameron, D. G. (1981) *Anal. Chem. 53*, 1454–1457.
5. Griffith, P. R. (ed.) (1978) *Transform techniques in chemistry*, Plenum Press, New York.
6. Byler, D. M. & Susi, H. (1986) *Biopolymers 25*, 469–487.
7. Surewicz, W. K. & Mantsch, H. H. (1988) *Biochim. Biophys. Acta 952*, 115–130.
8. Susi, H. & Byler, D. M. (1986) *Methods Enzymol. 130*, 290–311.
9. Castresana, J., Muga, A. & Arrondo, L. R. (1988) *Biochem. Biophys. Res. Commun. 152*, 69–75.
10. Arrondo, J. L., Muga, A., Castresana, J., Bernabeu, C. & Goni, F. M. (1989) *FEBS Lett. 252*, 118–120.
11. Arrondo, J. L., Muga, A., Prado, A. & Goni, F. M. (1988) *Mikrochim. Acta 1*, 385–388.
12. Mimms, L. T., Zampighi, G., Nozaki, Y., Tanford, C. & Reynolds, J. A. (1981) *Biochemistry 20*, 833–840.
13. Dorsett, D. L., Engel, A., Häner, M., Massalski, A. & Rosenbusch, J. P. (1983) *J. Mol. Biol. 165*, 701–710.
14. Heyn, M. P., Cherry, R. J. & Dencher, N. A. (1981) *Biochemistry 20*, 840–849.
15. Harrick, N. J. (1967) in *Internal reflection spectroscopy*, Wiley, New York.
16. Fringeli, U. P. & Günthard, H. H. (1981) in *Membrane spectroscopy* (Grell, E., ed.) pp 270–332, Springer-Verlag.
17. Levine, Y. K., Bailey, A. I. & Wilkins, M. H. F. (1968) *Nature 220*, 577–578.
18. Clark, N. A., Rothschild, K. J., Luippold, D. A. & Simon, B. A. (1980) *Biophys. J. 31*, 65–96.
19. Asher, S. A. & Pershan, P. S. (1979) *Biophys. J. 27*, 393–422.
20. MacNaughton, W., Snook, K. A., Caspi, E. & Franks, N. P. (1985) *Biochim. Biophys. Acta 818*, 132–148.
21. Tiede, D. M. (1985) *Biochim. Biophys. Acta 811*, 357–359.

22. Rothschild, K. J. & Clark, N. (1982) *Methods Enzymol. 88*, 696–714.
23. Cortijo, M., Alonso, A., Gomez-Fernandez, J. C. & Chapman, D. (1982) *J. Mol. Biol. 157*, 597–618.
24. Downer, N. W., Bruchman, T. J. & Hazzard, J. H. (1986) *J. Biol. Chem. 261*, 3640–3647.
25. Jackson, M., Haris, P. I. & Chapman, D. (1989) *Biochim. Biophys. Acta 998*, 75–79.
26. Krimm, S. & Bandekar, J. (1986) *Adv. Protein Chem. 38*, 181–364.
27. Cabiaux, V., Brasseur, R., Wattiez, R., Falmagne, P., Ruysschaert, J. M. & Goormaghtigh, E. (1989) *J. Biol. Chem. 264*, 4928–4938.
28. Gremlich, H. U., Fringeli, U. P. & Schwyzer, R. (1983) *Biochemistry 22*, 4257–4264.
29. Kauppinen, J. K., Moffat, D. J., Cameron, D. G. & Mantsch, H. H. (1981) *Appl. Opt. 20*, 1866–1879.
30. Jones, R. N. & Young, R. P. (1976) *Natl Res. Counc. Can. Bull. 13*, 25–39.
31. Goormaghtigh, E. & Ruysschaert, J. M. (1990) *in Molecular description of biological components* (Brasseur, R., ed.) CRC press, in the press.
32. Rothschild, K. J. & Clark, N. A. (1979) *Biophys. J. 25*, 473–488.
33. Levitt, M. & Greer, J. (1977) *J. Mol. Biol. 114*, 181–239.
34. Jap, B. K., Maestre, M. F., Hayward, S. B. & Glaeser, R. M. (1983) *Biophys. J. 43*, 81–89.
35. Nabedryk, E., Bardin, A. M. & Breton, J. (1985) *Biophys. J. 48*, 873–876.
36. Mao, D. & Wallace, B. A. (1984) *Biochemistry 23*, 2667–2673.
37. Shulte, T. H. & Marchesi, V. T. (1979) *Biochemistry 18*, 275–280.
38. Vogel, H. & Jähnig, F. (1986) *J. Mol. Biol. 190*, 191–199.
39. Lee, D. C., Hayward, J. A., Restall, C. J. & Chapman, D. (1985) *Biochemistry 24*, 4364–4373.
40. Chirgadze, Y. N., Brazhnikov, E. V. & Nevskaya, N. A. (1976) *J. Mol. Biol. 102*, 781–792.
41. Nevskaya, N. A. & Chirgadze, Y. N. (1976) *Biopolymers 15*, 637–648.
42. Blundell, T., Barlow, D., Borkakoti, N. & Thornton, J. (1983) *Nature 306*, 281–283.
43. Haris, P. I., Lee, D. C. & Chapman, D. (1986) *Biochim. Biophys. Acta 874*, 255–265.
44. Alvarez, J., Haris, P. I., Lee, D. C. & Chapman, D. (1987) *Biochim. Biophys. Acta 916*, 5–12.
45. Cabiaux, V., Goormaghtigh, E., Wattiez, R., Falmagne, R. & Ruysschaert, J. M. (1989) *Biochimie (Paris) 71*, 153–158.
46. Goormaghtigh, E., De Meutter, J., Vanloo, B., Brasseur, R., Rosseneu, M. & Ruysschaert, J. M. (1989) *Biochim. Biophys. Acta 1006*, 147–150.
47. Rothschild, K. J. & Clark, N. A. (1979) *Science 204*, 311–312.
48. Goormaghtigh, E., De Meutter, J., Szoka, F., Parente, R. & Ruysschaert, J. M. (1990) *Eur. J. Biochem.*, in the press.
49. Rothschild, K. J., Sanchez, R. & Clark, N. A. (1982) *Methods Enzymol. 88*, 696–715.
50. Yang, P. W., Stewart, L. C. & Mantsch, H. H. (1987) *Biochem. Biophys. Res. Commun. 145*, 298–302.
51. Nabedryk, E., Garvitato, R. M. & Breton, J. (1988) *Biophys. J. 53*, 671–676.
52. Kleffel, B., Garvitato, R. M., Baumeister, W. & Rosenbusch, J. P. (1985) *EMBO J. 4*, 1589–1592.
53. Fringeli, U. P. (1981) *Biophys. J. 34*, 173–187.
54. Henderson, R. & Unwin, P. N. T. (1975) *Nature 257*, 28–32.
55. Demel, R., Goormaghtigh, E. & de Kruijff, B. (1990) *Biochim. Biophys. Acta 1027*, 155–162.
56. Clark, N. A., Rothschild, K. J., Luippold, D. A. & Simon, B. A. (1980) *Biophys. J. 31*, 65–96.
57. Crowe, J. H., Spargo, B. J. & Crowe, L. M. (1987) *Proc. Natl Acad. Sci. USA 84*, 1537–1540.
58. Goormaghtigh, E., Ruysschaert, J. M. & Scarborough, G. A. (1988) *Prog. Clin. Biol. Res. 273*, 51–56.
59. Goormaghtigh, E., Martin, I., Vandenbranden, M., Brasseur, R. & Ruysschaert, J. M. (1989) *Biochem. Biophys. Res. Commun. 158*, 610–616.